Macular Structure and Function in Nonhuman Primate Experimental Glaucoma

Laura J. Wilsey, Juan Reynaud, Grant Cull, Claude F. Burgoyne, and Brad Fortune

Discoveries in Sight Research Laboratories, Devers Eye Institute and Legacy Research Institute, Legacy Health, Portland, Oregon, United States

Correspondence: Brad Fortune, Discoveries in Sight Research Laboratories, Devers Eye Institute and Legacy Research Institute, 1225 NE Second Avenue, Portland, 97232 OR, USA; bfortune@deverseye.org.

PURPOSE. To evaluate structure and function of macular retinal layers in nonhuman primate (NHP) experimental glaucoma (EG).

METHODS. Twenty-one NHP had longitudinal imaging of macular structure by SDOCT, 16 also had recordings of function by multifocal ERG. The average thickness over 15° was derived for seven individual SDOCT layers: macular nerve fiber layer (m-NFL), retinal ganglion cell layer (RGCL), inner plexiform layer (IPL), inner nuclear layer (INL), outer plexiform layer (OPL), outer nuclear layer+inner segments combined (ONL+IS), and outer segments (OS). Peripapillary RNFL thickness (ppRNFLT) was measured from a single circular B-scan with 12° diameter. Responses to a slow-sequence multifocal ERG (mfERG) stimulus (7F) were filtered (at 75 Hz) into low- and high-frequency components (LFC, HFC).

RESULTS. At final follow-up, significant structural loss occurred only in EG eyes and only for ppRNFLT ($-29 \pm 23\%$), m-NFL ($-17 \pm 16\%$), RGCL ($-22 \pm 15\%$), and IPL ($-19 \pm 14\%$); though there was also a small increase in OPL ($+6 \pm 7\%$) and ONL+IS ($4 \pm 4\%$) and a similar tendency for INL. Macular structural loss was correlated with ppRNFLT only for the NFL, RGCL and IPL ($R = 0.95$, 0.93 and 0.95, respectively, $P < 0.0001$). Significant functional loss occurred only for HFC and N2 in EG eyes. Significant longitudinal structure–function correlations ($P < 0.01$) were observed only in EG eyes and only for mfERG HFC and N2: HFC was correlated with ppRNFLT ($R = 0.69$), macular NFL ($R = 0.67$), RGCL ($R = 0.74$), and IPL ($R = 0.72$); N2 was correlated with RGCL ($R = 0.54$) and IPL ($R = 0.48$). High-frequency components amplitude change was inversely correlated with outer retinal thickness change ($= -0.66$).

CONCLUSIONS. Macular structural and functional losses are correlated and specific to ganglion cells over a wide range of EG severity. Outer retinal changes are likely due to inner retinal loss.

Keywords: glaucoma, macula, optical coherence tomography, electroretinography, ganglion cells

The extent to which outer retinal changes occur in human glaucoma and in experimental glaucoma (EG) models remains a controversial matter. One early anatomical study found approximately 23% reduction of nuclei in the photoreceptor (outer nuclear) layer within the central 20° of human eyes enucleated for relief from painful traumatic secondary angle-closure glaucoma.[1] In contrast, Kendall et al.[2] found no photoreceptor loss in human donor eyes with a history of POAG. Another anatomical study by Lei and colleagues[3] found no difference for outer nuclear layer cell counts overall, but up to 7% loss in the midperipheral retina that was spatially related to retinal ganglion cell (RGC) loss in human donor eyes with a history of POAG compared with age-matched control eyes. Nork and colleagues[4] reported "rare, patchy cone and rod losses" in glaucomatous human eyes and photoreceptor "swelling" based on subjective ratings by two of three observers. In a study of nonhuman primates (NHP) with end-stage EG in which RGC counts were reduced by greater than 80%, there was a reduction of parafoveal cones of only 3.5%.[5] Similarly, Frishman and colleagues[6] found little or no histologic evidence of abnormalities distal to the RGC layer in a study of NHP EG.

Function of the outer retina has been studied in human glaucoma using the electroretinogram (ERG, for a thorough review, see Holopigian et al.[7]). Velten and colleagues[8] reported that the amplitudes of scotopic ERG A-waves were reduced by approximately 30% in human patients with advanced, long-standing glaucomatous damage (mixture of primary, secondary, and low-tension glaucoma) as compared with controls that were, on average, approximately 13 years younger. Mitigating the age difference between study groups, Velten et al.[8] also showed that inter-ocular differences in A-wave amplitude were related to interocular differences in visual field damage. In contrast, Holopigian et al.[7] applied more advanced analyses to scotopic and photopic ERG A-waves and found no evidence of abnormal photoreceptor function in POAG.

Despite the fact that optical coherence tomography (OCT) has existed for well over a decade, enabling cross-sectional views and quantitative analysis of retinal anatomy, very few studies have evaluated the outer retina in glaucoma.[9] Using Fourier-domain OCT (FD-OCT), Wang and colleagues[10] evaluated individual retinal layer thicknesses across the macula in human eyes with a range of glaucomatous visual

field damage. They found an expected reduction in the thickness of the macular retinal nerve fiber layer (RNFL) and in the combined thickness of the RGC layer plus the inner plexiform layer (IPL), which were generally related to local visual field sensitivity, but no loss of outer retinal thickness.[10] Interestingly, an earlier study by Ishikawa and colleagues[11] using time domain OCT also found reduced thicknesses of macular inner retinal layers in glaucoma, but a 7% increase in the thickness of the "outer retinal complex" (combined thickness of the outer nuclear layer, inner and outer segments (IS/OS) of the photoreceptor layer). In a study using a combination of state-of-the-art adaptive-optics (AO) ultrahigh resolution FD-OCT and an AO-flood-illuminated fundus camera, Choi and colleagues[12] found that in areas where visual sensitivity was reduced from long-standing glaucoma, there were patchy dark areas within the otherwise regular cone photoreceptor mosaic, suggesting local loss of cones. These areas of reduced cone reflectivity observed in images from the AO-fundus camera corresponded to regions where measurements made by AO-FD-OCT revealed that the average length of cone OS was shortened and the variability increased.[12] Choi et al.[12] thought that shortening of cone OS could explain the patchy loss of cone density observed in the en face mosaics imaged by the AO-fundus camera, but also that "swelling" of cone OS could disrupt their waveguide properties and produce the same phenomenon. However, these findings are not specific to glaucoma as the same group demonstrated in several other forms of optic neuropathy whenever longstanding visual field loss was present.[13]

Perhaps because reliable segmentation of the numerous individual retinal layers visible in OCT scans is labor intensive, even fewer studies have evaluated outer retinal structure in EG models. Guo and colleagues[14] found a small decrease in RNFL thickness 3- and 8-weeks after chronic IOP elevation was induced unilaterally in rats, but they found no change in IPL thickness and a substantial progressive reduction of outer retinal thickness over that same period. In a study of NHP EG, Luo and colleagues[15] showed that localized measurements of macular inner retinal thickness (combined RGC+IPL) were modestly correlated to multifocal ERG measurements of RGC function in corresponding retinal locations but they did not evaluate outer retinal layers in that study. We have also recently reported that multifocal ERG measurements of RGC function averaged over wider spatial areas are correlated to both peripapillary RNFL thickness measurements made by OCT and to complete axon counts from the retrobulbar optic nerve in NHP EG.[16] In that study we found that other features of mfERG responses thought to reflect function of outer and middle retinal layers were not correlated to either peripapillary RNFL thickness or axon loss.[16]

Our purpose here was to measure macular retinal thickness layer-by-layer using longitudinal spectral-domain OCT (SDOCT) scans in NHP EG and compare those results to inner and outer retinal function measured in the macula by multifocal ERG.

METHODS

Subjects

The subjects of this study were 21 rhesus macaque monkeys (*Macaca mulatta*), 17 female and 4 male. At the start of study, their average age (±SD) was 11.3 ± 8.0 years, ranging 2.8 to 26.6 years and average weight was 6.0 ± 1.3 kg (range, 4.2–8.6 kg). This study was carried out in strict accordance with the recommendations in the Guide for the Care and Use of Laboratory Animals of the National Institutes of Health (Bethesda, MD, USA) and were approved and monitored by

the Institutional Animal Care and Use Committee (IACUC) at Legacy Health (USDA license 92-R-0002 and OLAW assurance A3234-01). All experimental methods and animal care procedures also adhered to the ARVO Statement for the Use of Animals in Ophthalmic and Vision Research.

Anesthesia

All experimental procedures began with induction of general anesthesia using ketamine (10–25 mg/kg IM) in combination with either xylazine (0.8–1.5 mg/kg IM), or midazolam (0.2 mg/kg IM), along with a single injection of atropine sulphate (0.05 mg/kg IM). Animals were then intubated with an endotracheal tube to breathe a mixture of 100% oxygen and air in order to maintain oxyhemoglobin saturation as close to 100% as possible. During ERG retinal function testing anesthesia was maintained using a combination of ketamine (5 mg/kg/hr IV) and xylazine (0.8 mg/kg/hr IM). In some cases, a constant rate infusion (1.2–3.0 mg/kg/hr) was used for IV ketamine delivery after a loading dose of 3.0 to 8.0 mg/kg. For all SDOCT imaging sessions anesthesia after initial induction was maintained using isoflurane gas (1%–2%) mixed with 100% oxygen and delivered via endotracheal tube. For SDOCT imaging, a clear, rigid gas permeable contact lens filled with 0.5% carboxymethylcellulose solution was placed over the apex of each cornea. In all sessions, IV fluids (lactated Ringer's solution, 10–20 mL/kg/hr) were administered via the saphenous vein, vital signs were monitored throughout and recorded every 10 to 15 minutes, including, heart rate, blood pressure, arterial oxyhemoglobin saturation, endtidal CO_2, and body temperature; body temperature was maintained at 37°C, heart rate above 75 per minute and oxygen saturation above 95%.

SDOCT Measurements of Peripapillary RNFL Thickness

All SDOCT scans were acquired using a Spectralis instrument as previously described (Heidelberg Engineering GmbH, Heidelberg, Germany)[16–20] 30 minutes after IOP was manometrically stabilized to 10 mm Hg. Peripapillary RNFL thickness was measured from a single high-resolution circular B-scan with a diameter of 12°, consisting of 1536 A-scans (Fig. 1). Nine to 16 individual sweeps were averaged in real time to comprise the final stored B-scan at each session. The position of the scan was centered on the optic nerve head (ONH) at the first imaging session and all follow-up scans were acquired at this same location using the instrument's automatic active eye tracking software. A trained technician masked to the purpose of this study manually corrected the accuracy of the instrument's native automated layer segmentations when the algorithm had obviously erred from the inner and outer borders of the RNFL to an adjacent layer (such as a refractive element in the vitreous instead of the internal limiting membrane, or to the outer border of the IPL instead of the RNFL).

SDOCT Scans of the Macula

Macula scans consisted of high-resolution B-scans oriented in a radial pattern centered on the fovea (Fig. 2). In most of the animals ($N = 14$) the macula scan pattern spanned 30° and contained 80 radial B-scans; in the others ($N = 7$), the scan pattern contained 48 radials and spanned 15°. In this study, we report the global spatial average for each macular layer and consider only the data from the central 15° (7.5° radius) in order to combine these groups and broaden the cohort. As
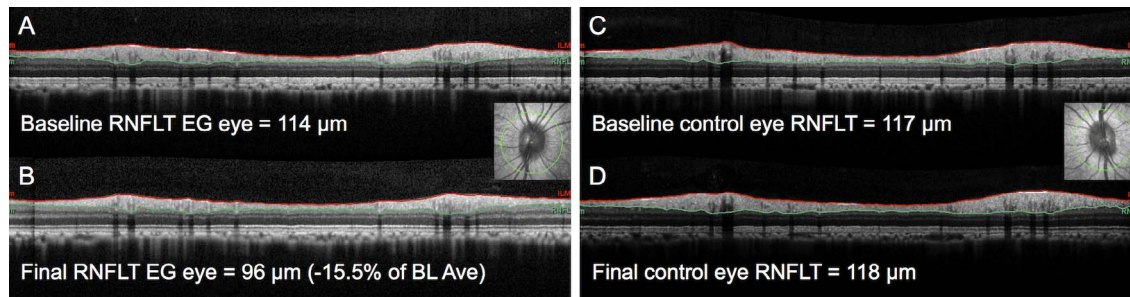
FIGURE 1. Peripapillary circular B-scans to measure peripapillary RNFLT. (**A**) Example for an individual EG eye at first baseline and (**B**) at the final imaging session. Results for the fellow control eye at the same time points (**C, D**). The B-scan location is indicated by the *green line* overlaid onto the infrared reflectance image *inset* in (**A, C**). *Red lines* show segmentations for anterior RNFL boundary (ILM); *green lines* show posterior boundary.

with the peripapillary scans, the instrument's automatic active eye tracking software was used to acquire all follow-up macula scans at the same location set during the first baseline.

The instrument's native automated layer segmentations were corrected where errant and the average thickness over 15° was derived for seven individual layers: macular nerve fiber layer (m-NFL), retinal ganglion cell layer (RGCL), IPL, inner nuclear layer (INL), outer plexiform layer (OPL), outer nuclear layer+inner segments combined (ONL+IS), and OS as shown in Figure 2.[21] Note, Henle's fibers were not distinguished from the ONL in this analysis.[22]
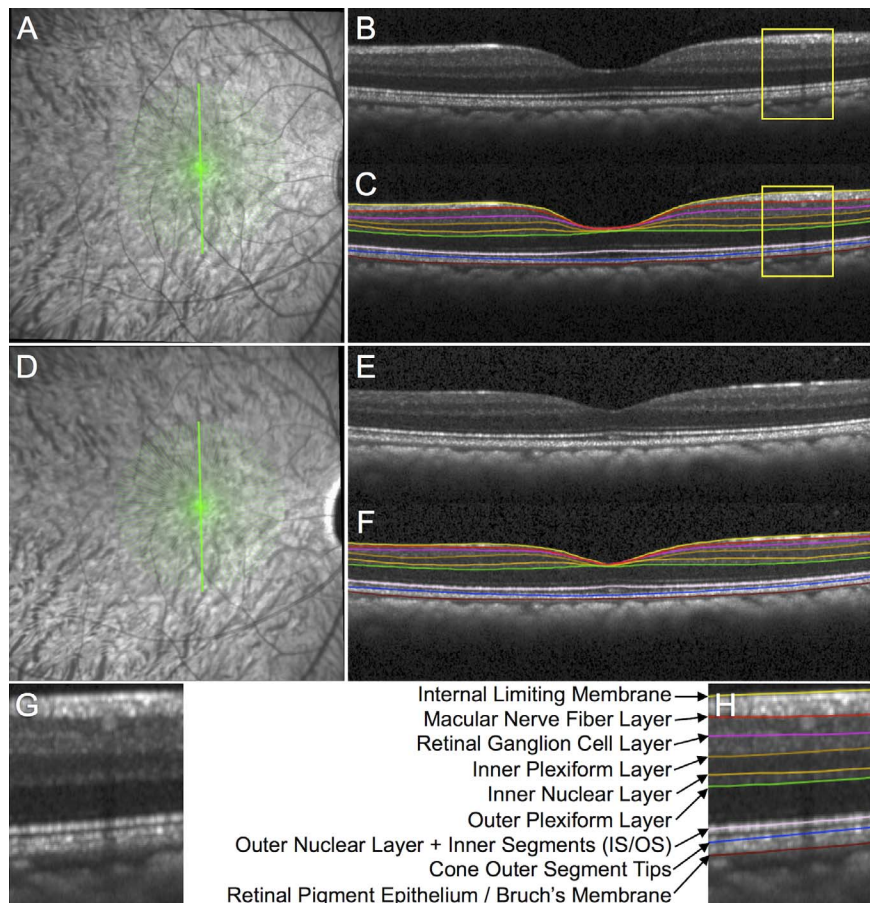

FIGURE 2. Spectral-domain OCT B-scan image segmentation to measure macular layer thicknesses. (**A**) The SDOCT radial 15° B-scan pattern is shown by the 48 *green lines* overlaid onto the infrared reflectance image at baseline in an individual EG eye. (**B**) Example of a single B-scan without segmentation and (**C**) with segmentation from the location indicated by the *bold green vertically oriented spoke* in (**A**). (**D**) Infrared reflectance image in the same EG eye at its final follow-up. (**E**) Vertical B-scan obtained at the final follow-up from the same location without segmentation and (**F**) with segmentation. (**G**) Magnified portion of the baseline B-scan from the *inset* indicated by the *yellow box* in (**B**) without segmentation and (**H**) with segmentation. The features segmented in each B-scan included the ILM and the posterior boundary of the following: m-NFL, RGCL, IPL, INL, OPL, and retinal pigment epithelium (Bruch's membrane). The center the reflectance bands associated with the IS/OS junction and the COST were also segmented, which served as the posterior boundaries of the combined outer nuclear layer + photoreceptor inner segments and the photoreceptor outer segments, respectively.[21]
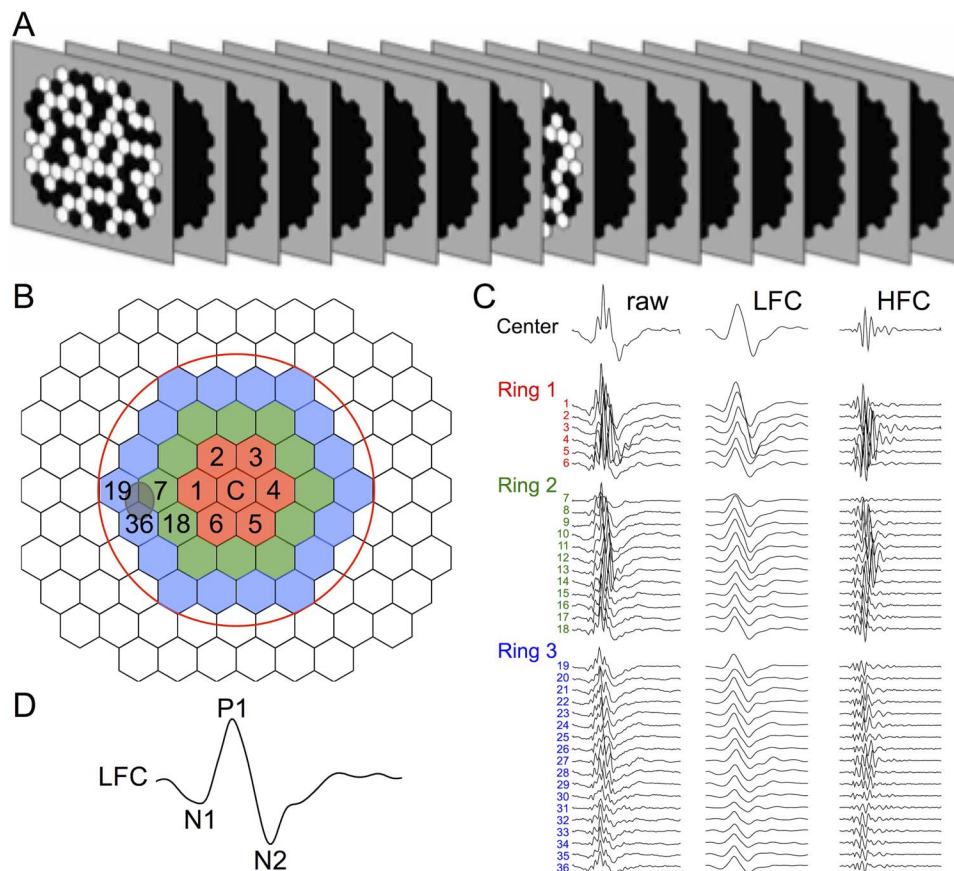
FIGURE 3. Multifocal ERG methods. (**A**) Schematic of slow-sequence mfERG stimulus with seven blank frames between each m-sequence step. Stimulus pattern was 103 hexagons over approximately 55°; mean luminance of m-steps: 100 cd/m²; contrast: approximately 99%; m-sequence exponent: 12; 8-minute recordings × 2 per session. In this study we analyzed the 37 responses from the area enclosed by the *red circle* in (**B**); which are shown for a healthy eye in (**C**) *color-coded* by *rings* around the central element and numbered by location. For each of the *three rings*, the responses are arranged down the column beginning with the response from the temporal field closest to the position of the "blind spot" (itself approximated by the *gray oval* overlapping elements 7, 19, 36), continuing around the ring through the superior field, nasal field, and inferior field. Each of the 37 central responses was filtered at 75 Hz into a LFC and HFC, as shown in *panel C* by the second and third column of traces, respectively. (**D**) The LFC features N1, P1, and N2 are labeled on the filtered response from the central element.

Multifocal ERG Measurements of Retinal Function

Retinal function was evaluated by multifocal ERG (mfERG).[16,17,23–25] Briefly, mfERGs were recorded using VERIS (Electro-Diagnostic Imaging, Inc., Redwood City, CA, USA). The mfERG stimulus consisted of 103 unscaled hexagonal elements subtending a total field size of approximately 55° (Fig. 3). The luminance of each hexagon was independently modulated between dark (1 cd/m²) and light (200 cd/m²) according to a pseudorandom, binary m-sequence. The temporal stimulation rate was slowed by insertion of seven dark frames into each m-sequence step ("7F"). The m-sequence exponent was set to 12, thus the total duration of each recording was 7 minutes 17 seconds. Signals were amplified (gain = 100,000), band-pass filtered (10–300 Hz; with an additional 60-Hz line filter), sampled at 1.2 kHz (i.e., sampling interval = 0.83 ms), and digitally stored for subsequent off-line analyses. Two such recordings were obtained for each eye at each time point and averaged.

From the average of the two recordings at each time point, a subset of local responses from the full array, limited to the central element and the three rings surrounding it (37 local responses in total), was processed to derive summary outcome parameters. A high-pass filter (5-pole, >75 Hz) was applied to each local mfERG response to extract the high frequency components (HFC). The low frequency component (LFC) of each response was represented as the raw response minus the HFC. The amplitude of the HFC was calculated as the root mean square (RMS) for the epoch between 0 and 80 ms of each filtered record. Peak amplitudes for LFC features were quantified as follows: the first negative feature (N1) was calculated as the maximum negative excursion from baseline in the epoch up to 30 ms; the amplitude of the first positivity (P1) was calculated as the voltage difference between the maximum peak and the N1 trough; and the second negativity (N2) was calculated as the difference between baseline and the minima from 30 to 80 ms The global average (of 37 response locations) for each parameter represented the measurement for each eye at each ERG session.

The HFC of mfERG responses to slow-sequence stimulation represent RGC function specifically, while the LFC features N1 and P1 reflect function of cone photoreceptors and cone bipolar cells.[15,23–26] Recent evidence indicates that the LFC feature N2 may also be affected by RGC loss in both NHP EG,[15,16] and clinical glaucoma,[27,28] and that it may be the mfERG homologue of the full-field ERG photopic negative response (PhNR; Viswanathan S, et al. *IOVS* 2009;50:ARVO E-Abstract 4758).[29–32]

Table 1. Average Thickness Values (μm) for Each Parameter at Each Time Point (±SD)

Group Average ± SD	ppRNFLT	m-NFL	GCL	IPL	INL	OPL	ONL+IS	OS
Control baseline 1	106.2 ± 9.2	24.9 ± 2.1	32.5 ± 2.4	32.3 ± 2.0	34.1 ± 1.9	24.7 ± 1.7	101.2 ± 5.2	29.6 ± 2.3
EG baseline 1	106.3 ± 8.3	25.5 ± 1.7	32.6 ± 2.4	32.6 ± 1.8	34.2 ± 1.5	24.8 ± 2.1	101.2 ± 4.0	29.9 ± 2.0
Control baseline 2	106.6 ± 9.7	24.6 ± 1.9	32.6 ± 3.0	32.0 ± 2.0	34.4 ± 2.0	24.3 ± 1.5	100.8 ± 4.8	28.4 ± 2.8
EG baseline 2	105.4 ± 10.2	24.9 ± 1.80	33.0 ± 2.6	32.0 ± 2.1	34.5 ± 1.8	24.3 ± 1.5	101.3 ± 4.4	28.3 ± 2.5
Control final	105.9 ± 10.5	25.7 ± 2.0	32.2 ± 2.9	31.5 ± 1.9	33.9 ± 1.8	24.5 ± 1.8	100.1 ± 4.8	29.1 ± 1.9
EG final	76.3 ± 27.7	21.0 ± 4.0	25.7 ± 5.2	26.3 ± 4.7	35.1 ± 2.2	25.9 ± 2.2	105.4 ± 6.5	29.7 ± 2.6

IOP Measurements

Intraocular pressure was measured in both eyes at the start of every session using a Tonopen XL (Reichert Technologies, Inc., Depew, NY, USA). The value recorded for each eye was the average of three successive measurements.

Experimental Design and Protocol

All 21 animals had longitudinal measurements of SDOCT and so data from all 21 contributed to the analysis of structural loss and structure–structure correlations, but only 15/21 had longitudinal mfERG measures of function, so analysis of functional loss and structure–function correlations was limited to data from those 15 animals. In all cases, each animal had a minimum of three weekly baseline recordings prior to laser treatment to induce chronic IOP elevation. This study includes data from the first two baseline sessions and from the final available session for each animal. After completion of the baseline series for each animal, argon laser photocoagulation was applied to the trabecular meshwork of one eye to induce chronic elevation of IOP.[33,34] Initially, 180° of the trabecular meshwork was treated in one session, then the remaining 180° was treated in a second session approximately 2 weeks later. If necessary, laser treatments were repeated in subsequent weeks (limited to a 90° sector) until an IOP elevation was first noted or if the initial post-laser IOP had returned to normal levels. The average number of laser treatments (±SD) was 5.0 ± 2.2 (range, 2–8).

After initiation of laser photocoagulation, the type of testing alternated weekly between SDOCT imaging one week and mfERG recordings the next week. Testing continued for each animal until its predefined sacrifice target had been reached. Specific targets for the EG stage when each animal was sacrificed were based on the primary study to which each animal was assigned and were predetermined based on those protocols. Thus, the EG stage at the final available session differed across animals, providing a relatively wide range of damage for analysis in this study.

Analysis and Statistics

All statistical analysis was performed using a commercial software package (Prism 5; GraphPad Software, Inc., La Jolla, CA, USA). Data from two baseline sessions was used to determine the repeatability coefficient[35] for each parameter in order to calculate the number of EG and control eyes that changed significantly ($P < 0.05$) between their baseline and the final session. For each parameter the magnitude of longitudinal change at the final session was assessed by Wilcoxon test with a criterion of P less than or equal to 0.001 to adjust for multiple comparisons. Pearson correlation coefficients were used to evaluate structure–structure and structure–function relationships; a conservative criterion was adopted to define significance ($P < 0.01$).

Results

Study Duration and IOP

The total study duration ranged from 7 to 28 months (average ± SD: 14.7 ± 6.6 months); the duration of post-laser follow-up ranged from 3 to 20 months (average ± SD: 10.0 ± 5.7). In the group of 21 EG eyes, mean IOP over the span of post-laser follow-up ranged from 10.4 to 35.8 mm Hg, with a group average of 21.1 ± 6.4 mm Hg. Mean IOP over the same period in the fellow control eyes was 11.4 ± 1.8 mm Hg. The peak IOP observed during post-laser follow-up period was 43.7 ± 11.9 in the EG eyes (range, 15.3–60.3 mm Hg) and 16.8 ± 2.8 mm Hg in control eyes.

Longitudinal Structural Changes and Structure–Structure Correlations

None of the structural parameters changed significantly between the first and second baseline time points in either EG or control eye groups (Table 1). There were also no significant differences between the average baseline values and the values at the final time point in control eyes (Fig. 4). In contrast, several structural parameters exhibited significant change between baseline and the final follow-up time point in the group of EG eyes as shown in Figure 4A. Longitudinal change for peripapillary RNFL thickness in EG eyes ranged from −2.5% to −78.3% (mean ± SD: −29.0 ± 23.4%, $P < 0.0001$). This represents a very wide range of EG severity, nearly the entire dynamic range of this parameter. For reference, the range of ONH neuroretinal rim thinning at the final time point in this group of 21 EG eyes measured using the OCT parameter minimum rim width (MRW)[36,37] was −4% to −89% relative to the baseline values. In this study, RNFL thickness is used as the metric of EG severity since it is more strongly correlated with complete optic nerve axon counts,[38] has lower measurement noise,[38] and has higher longitudinal signal-to-noise ratio than MRW or minimum rim area (MRA).[39]

There was also significant loss of thickness for macular inner retinal layers in EG eyes, including the m-NFL (−16.5 ± 15.9%, $P = 0.0001$), RGCL (21.7 ± 15.1%, $P < 0.0001$), and IPL (−18.5 ± 13.9%, $P < 0.0001$). However, we also observed a small but significant increase from baseline in EG eyes for the thickness of the OPL (5.8 ± 6.6%, $P = 0.001$) and the ONL+IS (4.1 ± 3.8%, $P = 0.0003$), but no significant change for the INL ($P = 0.05$) or OS thickness ($P = 0.15$).

We used the pairwise (intraeye) differences between the first and second baseline to calculate the repeatability coefficient for each parameter, and thus determine how many of the individual eyes exhibited significant change ($P < 0.05$) at the final time point. These results are listed in Table 2, which shows that 90% of the EG eyes had a significant reduction of peripapillary RNFL thickness, while a smaller proportion lost a significant amount of thickness of macular inner retinal layers. The data in Table 2 also show that nearly half of the EG eyes exhibited a significant increase in macular ONL+IS thickness.
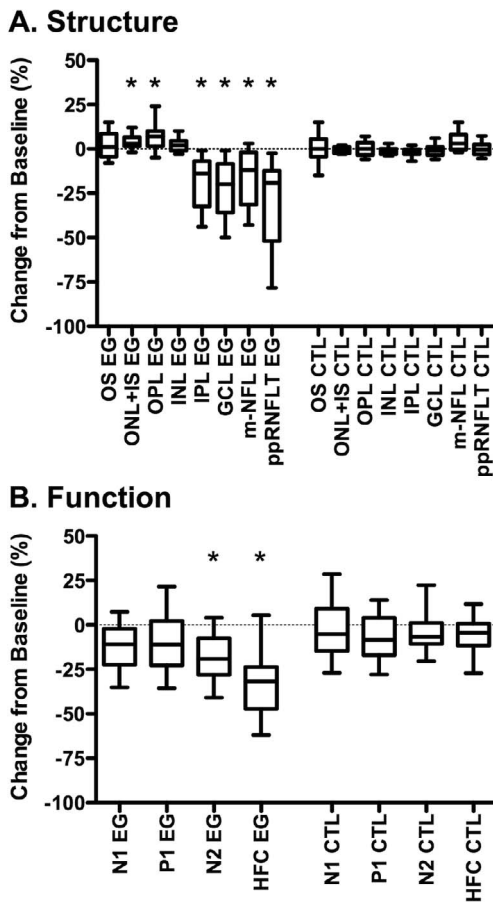
A. Structure

B. Function

FIGURE 4. Longitudinal changes in macular structure (**A**) and function (**B**). *Box plots* represent the distribution (median, interquartile range, extremes) of longitudinal change at the final session for each macular layer thickness (**A**) and mfERG parameter (**B**) in EG and fellow control eyes (CTL). Change is expressed as the difference from the average baseline value in the same eye: ([final value − baseline value]/baseline value) *P < 0.001. Peripapillary RNFL thickness is abbreviated as ppRNFLT.

FIGURE 5. Longitudinal changes in macular outer retinal thickness are inversely correlated to peripapillary RNFL thickness (ppRNFLT) loss (**A**) and to the degree of macular inner retinal thinning (**B**). Here, the combined outer retinal thickness was defined as the INL boundary to the COST line and the combined inner retinal thickness was defined as the sum of the m-NFL, RGCL, and IPL.

Macular inner retinal layer losses were strongly correlated with loss of peripapillary RNFL thickness as shown in Table 3. However, there was a significant inverse correlation between longitudinal changes for three of the four middle and outer retinal layers measured in the macula (INL, OPL, and ONL+IS) and the magnitude of peripapillary RNFL thickness loss. These data show that the relative degree of thickening in the INL, OPL, and ONL+IS is related to the severity of glaucomatous damage as indicated by thinning of the peripapillary RNFL.

Given the moderately strong inverse correlations between individual outer retinal layer thickness changes and peripapillary RNFL thickness loss, it was not surprising to find a
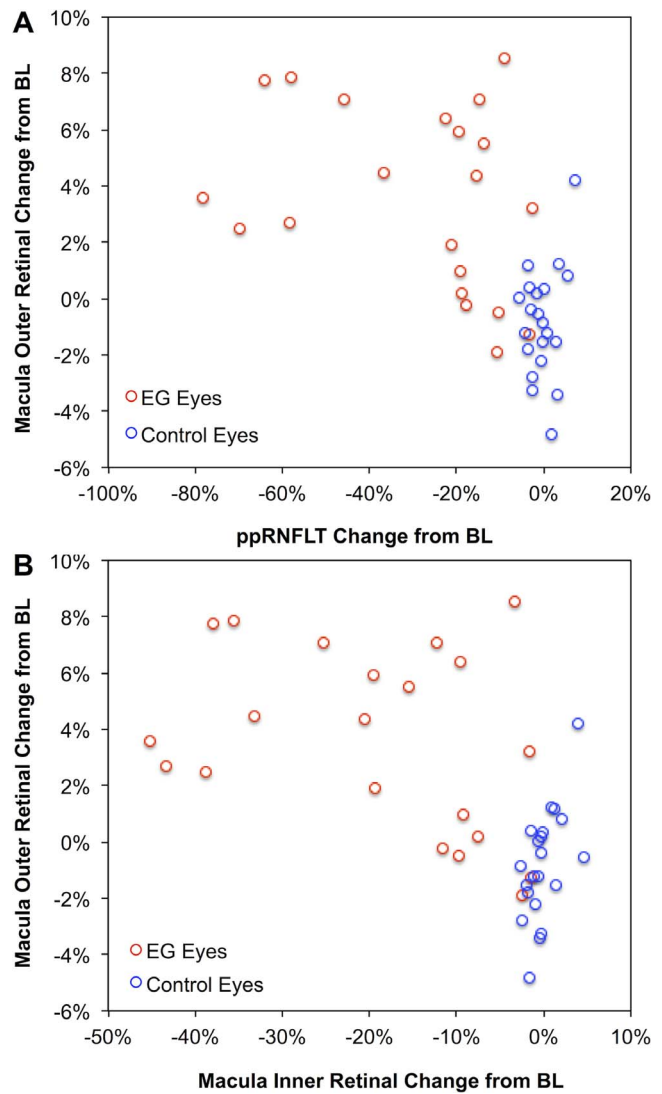
significant inverse correlation between changes in the combined outer retinal thickness (INL boundary to the cone outer segment tips, COST line) and overall EG damage severity measured by peripapillary RNFL thickness ($R = -0.56$, $P = 0.0001$, Fig. 5A). There was also a significant inverse correlation between changes in the combined outer retinal thickness and combined inner retinal thickness (m-NFL, RGCL,

TABLE 2. Proportion of Eyes Exhibiting Significant Longitudinal Structural Change From Baseline

% of N = 21 Eyes Change, P < 0.05	ppRNFLT	m-NFL	GCL	IPL	INL	OPL	ONL+IS	OS
EG decline	90%	43%	76%	81%	0%	0%	0%	0%
EG increase	0%	0%	0%	0%	*19%*	*24%*	*48%*	0%
CTL decline	0%	0%	0%	5%	0%	0%	5%	5%
CTL increase	5%	5%	0%	0%	0%	0%	0%	0%

Significant change at the final session was defined as exceeding the 95% range of baseline repeatability for that parameter. Values shown in bold font highlight the proportion of EG eyes exhibiting a significant decline, while values shown in bold italic font highlight the proportion of EG eyes exhibiting a significant increase of individual layer thickness.

TABLE 3. Longitudinal Structure–Structure Correlations: Macular Layer Thickness Change From Baseline Versus Peripapillary RNFLT Change From Baseline (Peripapillary RNFLT Serving as Measure of EG Severity)

vs. ppRNFLT	m-NFL	GCL	IPL	INL	OPL	ONL+IS	OS
Pearson R	**0.95**	**0.93**	**0.95**	**−0.54**	**−0.47**	**−0.51**	−0.10
P value	<0.0001	<0.0001	<0.0001	0.0002	0.0017	0.0005	0.5177

Values shown in bold font highlight strong, significant, direct correlations for inner retinal layers, while values shown in bold italic font highlight significant inverse correlations for outer and middle retinal layers.

and IPL; $R = -0.57$, $P < 0.0001$, Fig. 5B). For reference, the combined outer retinal thickness in EG eyes had increased by 4% over their baseline average ($P = 0.0001$) and was 5% thicker than the fellow control eyes at the final time point ($P < 0.0001$).

Longitudinal Functional Changes and Structure–Function Correlations

Significant functional loss occurred only in EG eyes and only for mfERG parameters HFC and N2 (Fig. 4B), though there was a tendency toward reduced N1 and P1 components as well, consistent with previous observations in a larger cohort.[16] Significant longitudinal structure-function correlations were observed only for mfERG HFC and N2 (Table 4). The magnitude of longitudinal mfERG HFC change was correlated with loss of peripapillary RNFL thickness ($R = 0.69$), macular NFL ($R = 0.67$), RGCL ($R = 0.74$), and IPL ($R = 0.72$); while mfERG N2 change was correlated with RGCL ($R = 0.56$) and IPL ($R = 0.52$) loss. Interestingly, there was a significant inverse correlation between loss of inner retinal function (mfERG HFC) and thickening of the combined outer retinal thickness (INL boundary to the cone outer segment tips, COST line, bottom row Table 4).

DISCUSSION

In this study we used SDOCT scans arranged in a dense radial pattern centered on the fovea to measure longitudinal changes in the thickness of individual retinal layers in a NHP model of EG. We observed predictable losses of macular inner retinal layers (m-NFL, GCL, and IPL) that were proportional to loss of peripapillary RNFL thickness, which is itself closely correlated to glaucomatous loss of axons from the orbital optic nerve.[16,38,40,41] We also found that thickness losses of macular inner retinal layers were correlated with loss of RGC-specific measures of function from the mfERG, similar to the results recently published by Luo and colleagues.[15]

However, this study was also focused on the outer retina, where we found little evidence of glaucomatous functional loss but an increased thickness of outer retinal layers (OPL and the combined ONL+IS) in EG eyes. Indeed, nearly half of the EG eyes exhibited a significant increase in macular ONL+IS thickness. Moreover, despite being a relatively small effect

(~4%-5%, on average), the degree of longitudinal outer retinal thickness increase was related to the severity of glaucomatous inner retinal damage, loss of peripapillary RNFL thickness, and loss of RGC function (mfERG HFC).

Very few studies have evaluated outer retinal layer thicknesses in human glaucoma. Wang and colleagues[10] found no loss of outer retinal thickness in their study. However, consistent with the results of our study, Ishikawa and colleagues[11] reported a 7% increase in the thickness of the "outer retinal complex" (combined thickness of the outer nuclear layer, inner, and outer segments of the photoreceptor layer). And although another study by Tan et al.[42] did not specifically report results for outer retinal thickness, one can infer from their results that macular outer retinal thickness was probably increased in glaucoma compared with controls because total macular retinal thickness provided poor discrimination despite clearly detectable inner retinal loss. One possible explanation for such results might be that the Müller cells could act as a scaffold to maintain retinal thickness to a degree (between the ILM and ELM) even while some of the layers collapse and so other layers may "spread" to fill the void. A similar mechanism has been suggested by Hood and colleagues[43] to explain their findings of increased RNFL thickness in patients with photoreceptor loss from retinitis pigmentosa.

Our finding of increased outer retinal thickness might also be consistent with results of Nork et al.,[4] who reported photoreceptor "swelling" in human glaucoma and in NHP EG. However, it is important to note that the difference between glaucomatous and control eyes reported by Nork et al.[4] was driven largely by 15 more glaucomatous eyes than control eyes in the group rated as "grade 3" (most swelling, see their Fig. 7) but it was never specified whether those 15 eyes were also among the oldest of all eyes studied (see Fig. 5 in Nork et al.[4]) and/or if those were the eyes with the longest duration of autolysis (see Fig. 6 in Nork et al.[4]). Both factors could have contributed to the outcome and neither factor was well balanced between glaucomatous and control samples.

Choi et al.[12] mentioned that while photoreceptor "swelling" could explain the patchy loss of cone density observed in the en face mosaics imaged by their AO-fundus camera, they also provided direct evidence from AO-ultrahigh resolution FD-OCT measurements to support the conclusion that shortened cone outer segments were contributing to the effect on the en

TABLE 4. Longitudinal Structure–Function Correlations: mfERG Parameter Change From Baseline Versus Peripapillary RNFL Thickness Change From Baseline (Top Row) and mfERG Parameter Change Versus Macular Layer Thickness Change (Rows 2-5)

mfERG vs. Structure	N1	P1	N2	HFC
Pearson R vs. ppRNFLT (P value)	0.35 (0.0527)	0.04 (0.8362)	0.40 (0.0232)	**0.69 (<0.0001)**
Pearson R vs. m-NFL (P value)	0.37 (0.0384)	0.10 (0.5931)	0.41 (0.0183)	**0.67 (<0.0001)**
Pearson R vs. GCL (P value)	0.37 (0.036)	0.17 (0.3577)	**0.54 (0.0015)**	**0.74 (<0.0001)**
Pearson R vs. IPL (P value)	0.40 (0.0239)	0.14 (0.4526)	**0.48 (0.0053)**	**0.72 (<0.0001)**
Pearson R vs. INL-COST (P value)	−0.23 (0.2137)	−0.02 (0.9052)	−0.37 (0.0347)	***−0.66 (<0.0001)***

Significant direct correlations for inner retinal layers are shown in bold font. A significant inverse correlation between inner retinal function and outer retinal thickness is highlighted in bold italic font.

face mosaic. We found no evidence that outer segments were shortened, at least not on average, in NHP eyes with a wide range of glaucomatous damage. However, our segmentation process aimed to bisect the COST reflectivity band (i.e., to identify the center of that peak in the longitudinal reflectivity profile) rather than to identify its anterior boundary, so it is possible that we could not detect subtle localized OS shortening as reported by Choi and colleagues[12] in glaucoma and other optic neuropathies.[13] The relatively thick and continuous COST band imaged in the macula by commercially available SDOCT such as we used in this study is thought to be produced by lateral blurring of the otherwise discrete points associated with individual cone OS tips, which are resolvable only by AO-OCT.[12,13,21] Thus, taken together, it appears there may be some subtle effects on the outer retina in glaucoma (and other optic neuropathies) that may best be explained by changes occurring after long-standing loss of inner retinal elements. It should also be noted that this conclusion is contrary to findings reported in a rodent model of EG.[14]

There are several limitations to this study, which may be important to consider. First, there is a mismatch between the areas used to obtain spatially averaged parameters of macular structure (15°) and function (30°) as well as a mismatch between each of those and the measure of glaucomatous damage severity we used (total average peripapillary RNFL thickness). Thus, it is possible that structure–structure and/or structure–function correlations might be even stronger than what we found in this study. However, Luo and colleagues[15] did analyze structure–function correlations based on more localized regions of inner retinal layers, but they reported generally lower correlation coefficients than what we found in similar comparisons. This might mean that the variability of parameters increases as measurement areas become more localized, and thus detracts from the apparent correlation strength. Since we had access to 30° of macular structural data in the majority of animals (14/21), we compared results based on 30° scans to those reported here for 15° scans and found no differences at all ($N = 14$, data not shown). This may reflect the fact that damage in this NHP model of EG is generally more diffuse than localized. Nevertheless, we intend in future studies to use dense raster-based scans of the macula to carefully determine individual structure–function maps for each eye based on axon bundle paths and use those to outline sectors for more localized comparisons.

Another limitation of this study is that it was based on data from only the baseline and final time points. It would be interesting to know when the outer retinal changes manifest during the longitudinal course of well-documented progression of inner retinal damage in each eye. Because the manual correction of image segmentations is extremely time consuming at present, detailed analysis of the longitudinal time course in each eye will require extensive additional work.

In summary, we found that macular retinal structural and functional losses are correlated and specific to RGCs over a wide range of EG severity. We also found that there was a small but significant increase of outer retinal layer thicknesses, which may represent "spreading" to fill the void of inner retinal loss. However, we did not find evidence of OS shortening (i.e., there was no change in the distance between the IS/OS junction and the COST line).

Disclosure: **L.J. Wilsey**, None; **J. Reynaud**, None; **G. Cull**, None; **C.F. Burgoyne**, Heidelberg Engineering, (F, C, R), GmbH (F, C, R); **B. Fortune**, None

References

1. Panda S, Jonas JB. Decreased photoreceptor count in human eyes with secondary angle-closure glaucoma. *Invest Ophthalmol Vis Sci*. 1992;33:2532–2536.

2. Kendell KR, Quigley HA, Kerrigan LA, Pease ME, Quigley EN. Primary open-angle glaucoma is not associated with photoreceptor loss. *Invest Ophthalmol Vis Sci*. 1995;36:200–205.

3. Lei Y, Garrahan N, Hermann B, et al. Quantification of retinal transneuronal degeneration in human glaucoma: a novel multiphoton-DAPI approach. *Invest Ophthalmol Vis Sci*. 2008;49:1940–1945.

4. Nork TM, Ver Hoeve JN, Poulsen GL, et al. Swelling and loss of photoreceptors in chronic human and experimental glaucomas. *Arch Ophthalmol*. 2000;118:235–245.

5. Wygnanski T, Desatnik H, Quigley HA, Glovinsky Y. Comparison of ganglion cell loss and cone loss in experimental glaucoma. *Am J Ophthalmol*. 1995;120:184–189.

6. Frishman LJ, Shen FF, Du L, et al. The scotopic electroretinogram of macaque after retinal ganglion cell loss from experimental glaucoma. *Invest Ophthalmol Vis Sci*. 1996;37: 125–141.

7. Holopigian K, Greenstein VC, Seiple W, Hood DC, Ritch R. Electrophysiologic assessment of photoreceptor function in patients with primary open-angle glaucoma. *J Glaucoma*. 2000;9:163–168.

8. Velten IM, Korth M, Horn FK. The a-wave of the dark adapted electroretinogram in glaucomas: are photoreceptors affected? *Br J Ophthalmol*. 2001;85:397–402.

9. Wong JJ, Chen TC, Shen LQ, Pasquale LR. Macular imaging for glaucoma using spectral-domain optical coherence tomography: a review. *Semin Ophthalmol*. 2012;27:160–166.

10. Wang M, Hood DC, Cho JS, et al. Measurement of local retinal ganglion cell layer thickness in patients with glaucoma using frequency-domain optical coherence tomography. *Arch Ophthalmol*. 2009;127:875–881.

11. Ishikawa H, Stein DM, Wollstein G, Beaton S, Fujimoto JG, Schuman JS. Macular segmentation with optical coherence tomography. *Invest Ophthalmol Vis Sci*. 2005;46:2012–2017.

12. Choi SS, Zawadzki RJ, Lim MC, et al. Evidence of outer retinal changes in glaucoma patients as revealed by ultrahigh-resolution in vivo retinal imaging. *Br J Ophthalmol*. 2011; 95:131–141.

13. Werner JS, Keltner JL, Zawadzki RJ, Choi SS. Outer retinal abnormalities associated with inner retinal pathology in nonglaucomatous and glaucomatous optic neuropathies. *Eye (Lond)*. 2011;25:279–289.

14. Guo L, Normando EM, Nizari S, Lara D, Cordeiro MF. Tracking longitudinal retinal changes in experimental ocular hypertension using the cSLO and spectral domain-OCT. *Invest Ophthalmol Vis Sci*. 2010;51:6504–6513.

15. Luo X, Patel NB, Rajagopalan LP, Harwerth RS, Frishman LJ. Relation between macular retinal ganglion cell/inner plexiform layer thickness and multifocal electroretinogram measures in experimental glaucoma. *Invest Ophthalmol Vis Sci*. 2014;55:4512–4524.

16. Fortune B, Cull G, Reynaud J, Wang L, Burgoyne CF. Relating retinal ganglion cell function and retinal nerve fiber layer (RNFL) retardance to progressive loss of RNFL thickness and optic nerve axons in experimental glaucoma. *Invest Ophthalmol Vis Sci*. 2015;56:3936–3944.

17. Fortune B, Burgoyne CF, Cull GA, Reynaud J, Wang L. Structural and functional abnormalities of retinal ganglion cells measured in vivo at the onset of optic nerve head surface change in experimental glaucoma. *Invest Ophthalmol Vis Sci.* 2012;53:3939–3950.

18. Fortune B, Burgoyne CF, Cull G, Reynaud J, Wang L. Onset and progression of peripapillary retinal nerve fiber layer (RNFL) retardance changes occur earlier than RNFL thickness changes in experimental glaucoma. *Invest Ophthalmol Vis Sci.* 2013; 54:5653–5661.

19. Fortune B, Reynaud J, Wang L, Burgoyne CF. Does optic nerve head surface topography change prior to loss of retinal nerve fiber layer thickness: a test of the site of injury hypothesis in experimental glaucoma. *PLoS One.* 2013;8:e77831.

20. Fortune B, Reynaud J, Cull G, Burgoyne CF, Wang L. The effect of age on optic nerve axon counts, SDOCT scan quality, and peripapillary retinal nerve fiber layer thickness measurements in Rhesus monkeys. *Transl Vis Sci Tech.* 2014;3(3):2.

21. Jonnal RS, Kocaoglu OP, Zawadzki RJ, Lee SH, Werner JS, Miller DT. The cellular origins of the outer retinal bands in optical coherence tomography images. *Invest Ophthalmol Vis Sci.* 2014;55:7904–7918.

22. Lujan BJ, Roorda A, Knighton RW, Carroll J. Revealing Henle's fiber layer using spectral domain optical coherence tomography. *Invest Ophthalmol Vis Sci.* 2011;52:1486–1492.

23. Fortune B, Wang L, Bui BV, Cull G, Dong J, Cioffi GA. Local ganglion cell contributions to the macaque electroretinogram revealed by experimental nerve fiber layer bundle defect. *Invest Ophthalmol Vis Sci.* 2003;44:4567–4579.

24. Fortune B, Wang L, Bui BV, Burgoyne CF, Cioffi GA. Idiopathic bilateral optic atrophy in the rhesus macaque. *Invest Ophthalmol Vis Sci.* 2005;46:3943–3956.

25. Fortune B, Cull GA, Burgoyne CF. Relative course of retinal nerve fiber layer birefringence and thickness and retinal function changes after optic nerve transection. *Invest Ophthalmol Vis Sci.* 2008;49:4444–4452.

26. Rangaswamy NV, Zhou W, Harwerth RS, Frishman LJ. Effect of experimental glaucoma in primates on oscillatory potentials of the slow-sequence mfERG. *Invest Ophthalmol Vis Sci.* 2006; 47:753–767.

27. Kaneko M, Machida S, Hoshi Y, Kurosaka D. Alterations of photopic negative response of multifocal electroretinogram in patients with glaucoma. *Curr Eye Res.* 2015;40:77–86.

28. Kato F, Miura G, Shirato S, Sato E, Yamamoto S. Correlation between N2 amplitude of multifocal ERGs and retinal sensitivity and retinal nerve fiber layer thickness in glaucomatous eyes. *Doc Ophthalmol.* 2015;131:197–206.

29. Viswanathan S, Frishman LJ, Robson JG, Harwerth RS, Smith EL III. The photopic negative response of the macaque electroretinogram: reduction by experimental glaucoma. *Invest Ophthalmol Vis Sci.* 1999;40:1124–1136.

30. Viswanathan S, Frishman LJ, Robson JG, Walters JW. The photopic negative response of the flash electroretinogram in primary open angle glaucoma. *Invest Ophthalmol Vis Sci.* 2001;42:514–522.

31. Rangaswamy NV, Frishman LJ, Dorotheo EU, Schiffman JS, Bahrani HM, Tang RA. Photopic ERGs in patients with optic neuropathies: comparison with primate ERGs after pharmacologic blockade of inner retina. *Invest Ophthalmol Vis Sci.* 2004;45:3827–3837.

32. Machida S. Clinical applications of the photopic negative response to optic nerve and retinal diseases. *J Ophthalmol.* 2012;2012:397178.

33. Gaasterland D, Kupfer C. Experimental glaucoma in the rhesus monkey. *Invest Ophthalmol.* 1974;13:455–457.

34. Quigley HA, Hohman RM. Laser energy levels for trabecular meshwork damage in the primate eye. *Invest Ophthalmol Vis Sci.* 1983;24:1305–1307.

35. Bland JM, Altman DG. Measuring agreement in method comparison studies. *Stat Methods Med Res.* 1999;8:135–160.

36. Strouthidis NG, Fortune B, Yang H, Sigal IA, Burgoyne CF. Longitudinal change detected by spectral domain optical coherence tomography in the optic nerve head and peripapillary retina in experimental glaucoma. *Invest Ophthalmol Vis Sci.* 2011;52:1206–1219.

37. He L, Yang H, Gardiner SK, et al. Longitudinal detection of optic nerve head changes by spectral domain optical coherence tomography in early experimental glaucoma. *Invest Ophthalmol Vis Sci.* 2014;55:574–586.

38. Fortune B, Hardin C, Reynaud J, et al. Comparing optic nerve head rim width, rim area and peripapillary retinal nerve fiber layer thickness to axon count in experimental glaucoma. *Invest Ophthalmol Vis Sci.* In press.

39. Gardiner SK, Boey PY, Yang H, Fortune B, Burgoyne CF, Demirel S. Structural measurements for monitoring change in glaucoma: comparing retinal nerve fiber layer thickness with minimum rim width and area. *Invest Ophthalmol Vis Sci.* 2015;56:6886–6891.

40. Cull GA, Reynaud J, Wang L, Cioffi GA, Burgoyne CF, Fortune B. Relationship between orbital optic nerve axon counts and retinal nerve fiber layer thickness measured by spectral domain optical coherence tomography. *Invest Ophthalmol Vis Sci.* 2012;53:7766–7773.

41. Cull GA, Reynaud J, Wang L, Cioffi GA, Burgoyne CF, Fortune B. Erratum in: "relationship between orbital optic nerve axon counts and retinal nerve fiber layer thickness measured by spectral domain optical coherence tomography." *Invest Ophthalmol Vis Sci.* 2014;55:2619–2620.

42. Tan O, Chopra V, Lu AT, et al. Detection of macular ganglion cell loss in glaucoma by Fourier-domain optical coherence tomography. *Ophthalmology.* 2009;116:2305–2314, e2301–e2302.

43. Hood DC, Lin CE, Lazow MA, Locke KG, Zhang X, Birch DG. Thickness of receptor and post-receptor retinal layers in patients with retinitis pigmentosa measured with frequency-domain optical coherence tomography. *Invest Ophthalmol Vis Sci.* 2009;50:2328–2336.